Accepted Manuscript

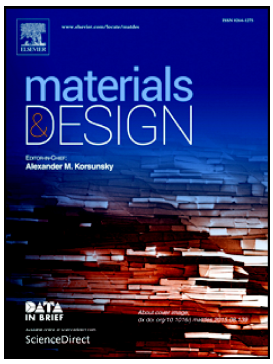

Fatigue performance of fused filament fabrication PLA specimens

Giovanni Gomez-Gras, Ramón Jerez-Mesa, J. Antonio Travieso-Rodriguez, Jordi Lluma-Fuentes

PII:	S0264-1275(17)31103-6
DOI:	doi:10.1016/j.matdes.2017.11.072
Reference:	JMADE 3549
To appear in:	*Materials & Design*
Received date:	17 November 2017
Revised date:	28 November 2017
Accepted date:	30 November 2017

Please cite this article as: Giovanni Gomez-Gras, Ramón Jerez-Mesa, J. Antonio Travieso-Rodriguez, Jordi Lluma-Fuentes , Fatigue performance of fused filament fabrication PLA specimens. The address for the corresponding author was captured as affiliation for all authors. Please check if appropriate. Jmade(2017), doi:10.1016/j.matdes.2017.11.072

Fatigue performance of fused filament fabrication PLA specimens

Authors:

1. Giovanni Gomez-Gras
   Insititut Químic de Sarrià. Universitat Ramon Llull, Industrial Engineering Department. Address: Via Augusta, 390. 08017 Barcelona, Spain. Tel.: (+34)932672124. Mail: giovanni.gomez@iqs.edu

2. Ramón Jerez-Mesa
   Universitat Politècnica de Catalunya. Escola d'Enginyeria de Barcelona Est. Mechanical Engineering Department. Address: Avinguda d'Eduard Maristany, 10-14. 08019 Barcelona, Spain. Tel.: (+34)934137431. Mail: ramon.jerez@upc.edu

3. J. Antonio Travieso-Rodriguez
   Universitat Politècnica de Catalunya. Escola d'Enginyeria de Barcelona Est. Mechanical Engineering Department. Address: Avinguda d'Eduard Maristany, 10-14. 08019 Barcelona, Spain. Tel.:(+34)934137338. Mail: antonio.travieso@upc.edu (corresponding author)

4. Jordi Lluma-Fuentes
   Universitat Politècnica de Catalunya. Escola d'Enginyeria de Barcelona Est. Materials Science and Metallurgical Engineering Department, Address: Avinguda d'Eduard Maristany, 10-14. 08019 Barcelona, Spain. Tel.:(+34)934137296. Mail: jordi.lluma@upc.edu

Abstract

This paper aims to analyze the fatigue response of PLA parts manufactured through fused filament fabrication (FFF). The influence of four factors (layer height, fill density, nozzle diameter and velocity) on the fatigue performance of cylindrical specimens is studied through an L27 Taguchi experimental design. This design is run for two different infills: linear and honeycomb. Specimens have been tested on a rotating fatigue bending machine. The optimal set of parameters and levels resulting in the highest number of cycles to failure have been determined, and implemented to manufacture a second set of specimens, which have been tested at different stress levels to represent the Wöhler curve. Fill density proves to be the most influential parameter on fatigue life, followed by layer height. The tests undertaken to represent the Wöhler curve revealed that 35.8 MPa can be considered as a lower threshold of the endurance limit for this kind of specimens. This value can be useful to use these devices to manufacture human implants, as PLA is a biocompatible material. The main novelty of this paper is that no previous fatigue life assessment of PLA parts manufactured through FFF has been developed.

Keywords: additive manufacturing, 3D printing, fused filament fabrication, fatigue, PLA

Nomenclature

FFF - fused filament fabrication

FDM - fused deposition modelling

PLA - polylactic acid

ABS - acrylonitrile butadiene styrene

DOE - statistical design of experiments

ANOVA - analysis of variance

1. Introduction

3D printing is a generic term used to define any kind of additive or layered manufacturing process, that is, a group of techniques used to obtain final parts or prototypes in a short period from a digital design by progressive addition of a raw material [1]. Of all possible technologies through which 3D printers can perform the manufacturing process, fused filament fabrication (FFF), also known as fused deposition modelling (FDM), is the most extended one. Through this technology, the raw material is a filament, usually of PLA or ABS, which is progressively taken into a heated extruder (Fig. 1). As the raw material is pressed downwards, its temperature rises over its glass transition temperature, thus becoming suitable for extrusion through a nozzle of a controlled diameter [2]. The semimelted material is deposited on the previously laid layer, so that both hot fibers of material are joint through a local sintering process of neck growth, as described in [3]. The desired shape is obtained by a numerical control based code which moves the extruder along the plane on which manufacturing takes place for each layer.

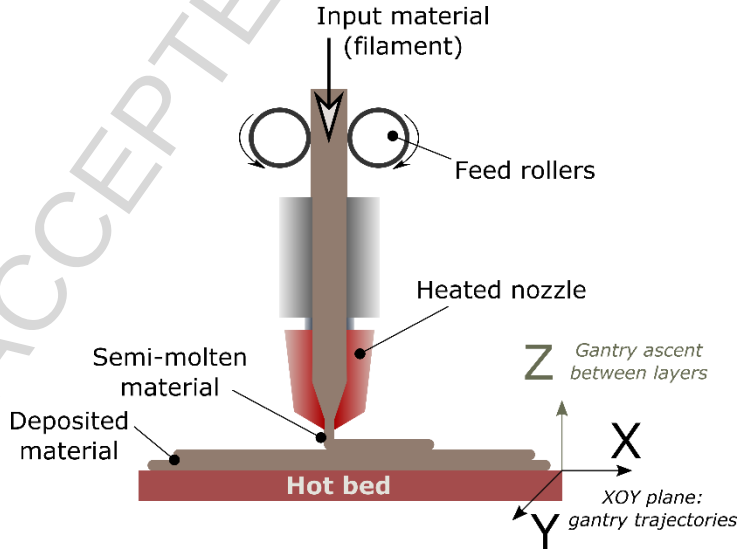

Fig. 1 Schematic representation of a fused deposition modelling system

The mechanical behavior of 3D printed parts is one of the most difficult properties to define in this kind of parts, for two main reasons. Firstly, because of the high number of parameters to control during the additive process, which makes it complex to analyze.

Secondly, because of the high anisotropy that this kind of parts show when tested, which is defined by their manufacturing history, as the resistance of the raw material and the cohesive forces between bonded layers interact in a complex way [4]. Consequently, parts manufactured through additive processes show a preferential bearing direction, normally the one along which the material is deposited [5].

This paper focuses on the response of 3D printed specimens subjected to dynamic stresses, considering the influence of different factors. One of them is the manufacturing orientation, which determines the preferential stress carrying direction. Previous works show that this direction should ideally coincide with the expected in-service loads of the part to maximize its mechanical performance [6-10]. Not only are parts manufactured through additive processes highly anisotropic, but there is also a great discrepancy between internal cohesion forces among the polymer chains, and inter-layer forces, which account for the cohesion of the whole workpiece [11]. For this reason, the decision on building orientation should be taken regarding the expected in-service loads of the workpiece. Fig. 2 shows two different 3D printed specimens subjected to axial loads. At the one manufactured along the *z* axis (A), the load is aligned with the preferential carrying direction. Therefore, the inner forces of the raw material polymer define the carrying capacity of the specimen. On the contrary, the (B) specimen is expected to have a lower resistance, as the cohesive forces between filaments are much lower than the polymer inner forces, which drastically decreases its carrying capacity.

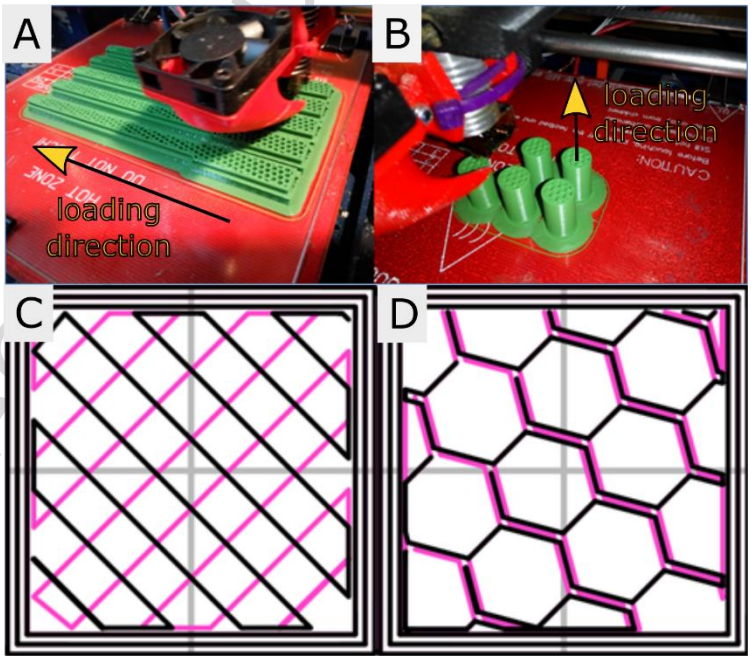

Fig. 2 A. Printed specimens loaded along the preferential axis. **B.** Loaded along the weak axis. **C.** Rectilinear infill **D.** Honeycomb infill.

Researchers have observed this behavior in parts manufactured through other additive manufacturing processes such as Stereolitography [12-13], Selective Laser Sintering [14-17], or Layered Object Manufacturing [18]. This behavior has also been observed in metallic specimens [19-20].

The second factor considered in this paper as influential is layer height, that is, the longitudinal value that the extruder rises between the deposition of one layer and the next one. As layer height decreases, parts show a higher cohesion among layers, due to an increase in surface contact between filaments, and the consequent increase in heat transport mechanisms, which favor neck growth among them [21]. It also has a remarkable influence on surface roughness and unitary cost of a part, as the addition of more layers implies a higher material consumption for a fixed defined volume [22-23].

The infill strategy is composed of two different terms, namely the fill density and the pattern. The first one has showed a relevant effect on the stiffness of 3D printed part, which increases with the decrease of the gap between rasters. This effect can be explained by the positive effect of a higher density of material inside the part volume. As for the infill pattern, it refers to the path that the extruder follows in order to fill each layer. These patterns are usually defined at the slicer software which generates the numerical control interpolations. The rectilinear one is the most generalized approach, as it allows to form the part by piling layers composed of parallel linear rasters, while the direction of those rasters is alternatively changed in 90-degrees (Fig. 2C). On the other hand, the honeycomb strategy (Fig. 2D), has also shown good results in term of mechanical properties [24]. For this reason, both infill patterns have been chosen for this paper.

Other parameters defining the manufacturing process through FFF are the nozzle diameter, which is the nominal expected diameter of the extruded filament, and the extrusion velocity. Both of them show a relevant effect on resistance, but also on other aspects of part quality as surface roughness and part distortion due to residual thermal stresses [25-26]. In effect, they are highly influential on heat transfer mechanisms, and must be controlled in order to keep the temperature of the manufactured specimen as constant as possible [27].

The manufacturing strategy, executed by the ISO code which commands the different 3D printer functions, is programmed by a slicer software from the only input of an STL model and the decided parameters. Although some authors have published technical recommendations to improve the quality of 3D printed parts [28,29], there is no agreement on the optimal level of the different printing parameters to take into account. For this reason, this investigation has been developed to expand the knowledge about printing parameters, focusing on fatigue behavior as response variable.

The fatigue performance of rapid manufactured parts has been scarcely tackled in the bibliography. The most numerous references are found for laser sintered metal specimens [30-32]. However, very few references have been found dealing with fatigue behavior of PLA specimens. For instance, Afrose et al. (2016) [33] only considered the manufacturing orientation as a factor of study, and found that specimens built at 45 degrees presented the highest fatigue life expected for every stress level tested.

The detected lack of references about the influence of other parameters on fatigue life, as well as a comprehensive study about fatigue behavior of FFF PLA parts has motivated the research presented in this paper. One preferential building orientation has been prefixed for the manufacturing of specimens, and two different infill patterns have been tested. For each of them, a Taguchi orthogonal array was designed and applied, taking into account four factors at three levels: layer height, fill density, nozzle diameter and printing velocity. The best combination of levels and values is obtained, and a second set of specimens are tested subjected to different stresses, to the S-N curve associated with the selected manufacturing strategy.

2. Materials and methods

2.1 Taguchi experimental design

Table 1 shows the factors and selected levels with which the Taguchi experimental design is to be developed. This technique allows to reduce the number of runs albeit including a high number of factors and tested levels. It has been successfully applied to other experimental research focused on FDM parts [34]. These factors have been selected for their high influence on mechanical properties of rapid manufactured parts, as reviewed in the introduction, and their levels have been selected according to previous experience and observations in a preliminary experimental phase.

Table 1 Factors and levels used for the DOE

Factor	Code	Level			Unit
		1	2	3	
Layer height	A	0,1	0,2	0,3	mm
Nozzle diameter	B	0,3	0,4	0,5	mm

Fill density	C	25	50	75	%
Printing velocity	D	25	30	35	mm/min

An L27 Taguchi orthogonal array has been selected to conduct the experimental phase (Table 2). It allows to analyze the influence of the selected four parameters on the response variable, that is, the cycles to failure presented by specimens at a rotating bending test. This approach leaves enough degrees of freedom to include in the analysis the influence of second order interactions among three of them [35]. Of all four factors, the printing velocity has been discarded for interactions analysis, as is expected to be the least significant, in view of the results of preliminary tests.

Table 2 L27 Taguchi orthogonal array for the DOE. This experimental planning has been performed for two sets of specimens with a different infill pattern.

# run	Layer height	Nozzle diameter	Fill density	Printing velocity
1	0.1	0.3	25	25
2	0.1	0.3	50	30
3	0.1	0.3	75	35
4	0.1	0.4	25	30
5	0.1	0.4	50	35
6	0.1	0.4	75	25
7	0.1	0.5	25	35
8	0.1	0.5	50	25
9	0.1	0.5	75	30
10	0.2	0.3	25	30
11	0.2	0.3	50	35
12	0.2	0.3	75	25
13	0.2	0.4	25	35
14	0.2	0.4	50	25
15	0.2	0.4	75	30
16	0.2	0.5	25	25
17	0.2	0.5	50	30
18	0.2	0.5	75	35
19	0.3	0.3	25	35

20	0.3	0.3	50	25
21	0.3	0.3	75	30
22	0.3	0.4	25	25
23	0.3	0.4	50	30
24	0.3	0.4	75	35
25	0.3	0.5	25	30
26	0.3	0.5	50	35
27	0.3	0.5	75	25

The building orientation has not been included as an experimental factor, and the already assumed as preferential bearing direction, that is, the axial direction along the specimen, has been selected to manufacture specimens. The infill pattern is to be studied but has not been included in the experimental design, as only two patterns want to be assessed: rectilinear and honeycomb. The experimental design has been therefore repeated once for each one of them. Consequently, 54 different types of specimens were manufactured. For each one, five specimens were manufactured, to confirm the repeatability of the obtained results, and provide the results of statistical significance.

2.2 Specimen manufacture

Specimens have been manufactured using a Prusa i3 Steel 3D printer. The parameters that are not object of study have been kept constant among different specimens. All specimens have been manufactured with 2 external perimeters, 5-mm brim support and three solid layers at the bottom of the specimen. At the bottom layers, the printing has been supported with an rectilinear gridded structure that was removed before the fatigue testing.

There is no a specific standard focusing on fatigue testing of plastic laminated materials. Therefore, special specimens have been designed, adapting their dimensions to the possibilities offered by the testing machine (Fig. 3). However, the design of the specimens are not in total disagreement with the ASTM D7774 standard [36], that regulates the test method for flexural fatigue properties of plastics.

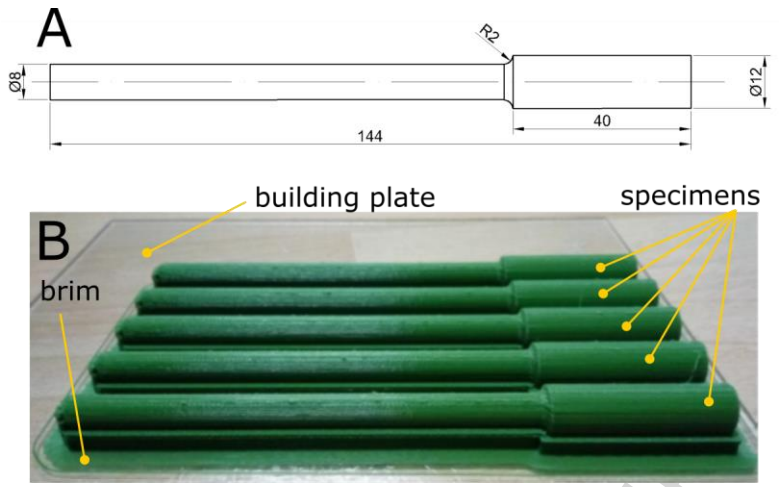

Fig. 3 A. Specimens used for the fatigue tests. **B.** Overview of five specimens manufactured, all of them sharing the same manufacturing parameters.

2.3 Experimental setup

The whole experimental setup is shown at Fig. 4. A GUNT WP 140 rotating bending stress machine has been used for the experiments. The specimens were clamped to the chuck of the machine, and spindled at a speed of 2800 min^{-1}. The fluctuating stress was forced by the application of a concentrated load at the end of the beam, which was regulated through a load cell installed at the loading mechanism. For the first experimental phase, a 15 N force was applied at all specimens. During the second phase, where the tests to draw the Wöhler curve were performed, this force wass varied from 10 to 22 N taking discrete steps. The number of cycles that each specimen endured was registered by a digital revolutions counter.

A PCE-TC 3 thermographic camera was also installed to monitor the evolution of the temperature of the specimen at the stress concentrator area, to assess if there is a relevant thermal effect. Its sensitivity is 0.15ºC and precision is of ±2 ºC. Both values are considered admissible for this kind of study, where the temperature can be considered as secondary to characterize the process.

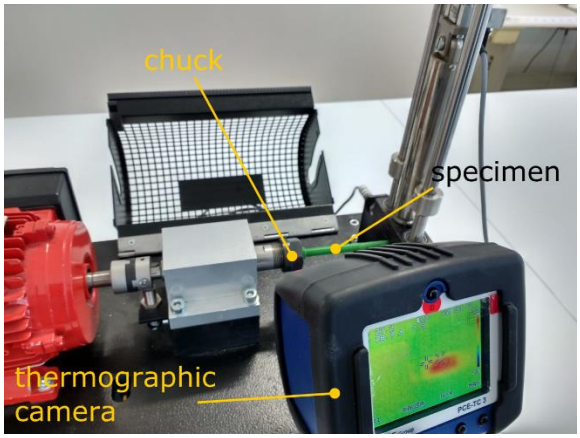

Fig. 4. Overview of the experimental setup.

3. Results and discussion

3.1 Comparative results

Once all experiments were developed and cycles to failure counted, outliers inside each set of data for each printing condition and both infill patters were identified and discarded by applying the Chauvenet's criterion. As fatigue assessment is a purely experimental study, this previous analysis was performed so that the statistical analysis of the Taguchi DOE would not be biased. Figure 5 shows the average value of number of cycles to failure found for each printing condition, along with the standard deviation after eliminating dubious data. The results show that honeycomb specimens allowed longer lifespans, for almost all printing conditions. Therefore, this type of infill is recommended for parts expected to be subjected to alternating loads.

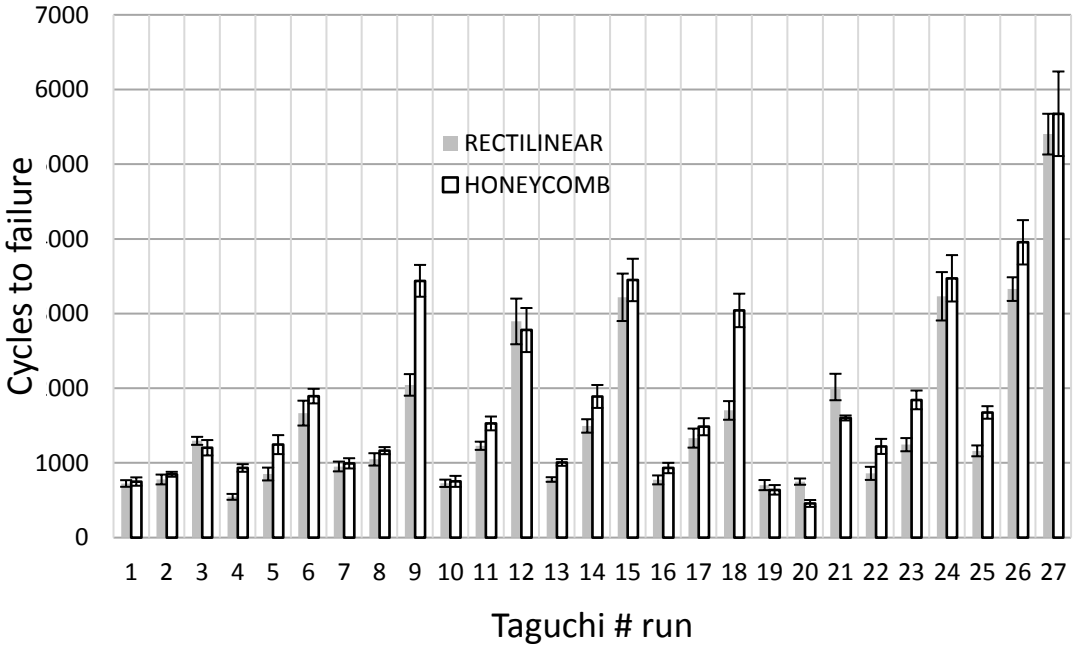

Fig. 5 Comparison between the average number of cycles to failure between rectilinear filled and honeycomb specimens for all printing conditions at the Taguchi array.

The surface temperatures were recorded during each whole experiment, and the value at the moment of failure was extracted. All specimens registered temperatures from 42.5ºC to 60.5ºC, and no pattern or relation with the printing conditions observed. As all of them are under the glass transition temperature of PLA, fatigue crack and failure cannot be associated with any kind of thermal effect, and no further disquisition was undertaken.

3.2 Analysis of variance

An analysis of variance (ANOVA) was performed on the dataset presented by both Taguchi experimental arrays executed for each infill pattern. Once calculated the associated linear model, an Anderson Darling test to check the residual normality hypothesis of both sets of values was performed. The p-values were in both cases higher than a significance level of 5%, thus leading to accept the normality hypothesis. Fig. 6 shows the main effects plot for both infills. In both cases, the fill density is the most influential parameter. It is noticeable that the influence is not linear, as the increase in fatigue life is stronger when the part is filled from 50% to 75% of the nominal volume, in comparison to the improvement when increasing from 25% to 75%. The nozzle diameter and layer height are the next two most influential parameters, but their relative position changes depending on the infill pattern. Rectilinear specimens showed a higher influence of layer height on the result, whereas the nozzle diameter was more influential on the cycles to failure in honeycomb specimens. Velocity showed no significant influence on the results, probably because similar values were analyzed and included in the DOE. The analysis of signal-to-noise ratios show a similar pattern, thus concluding that the most influential factors show also the highest robustness.

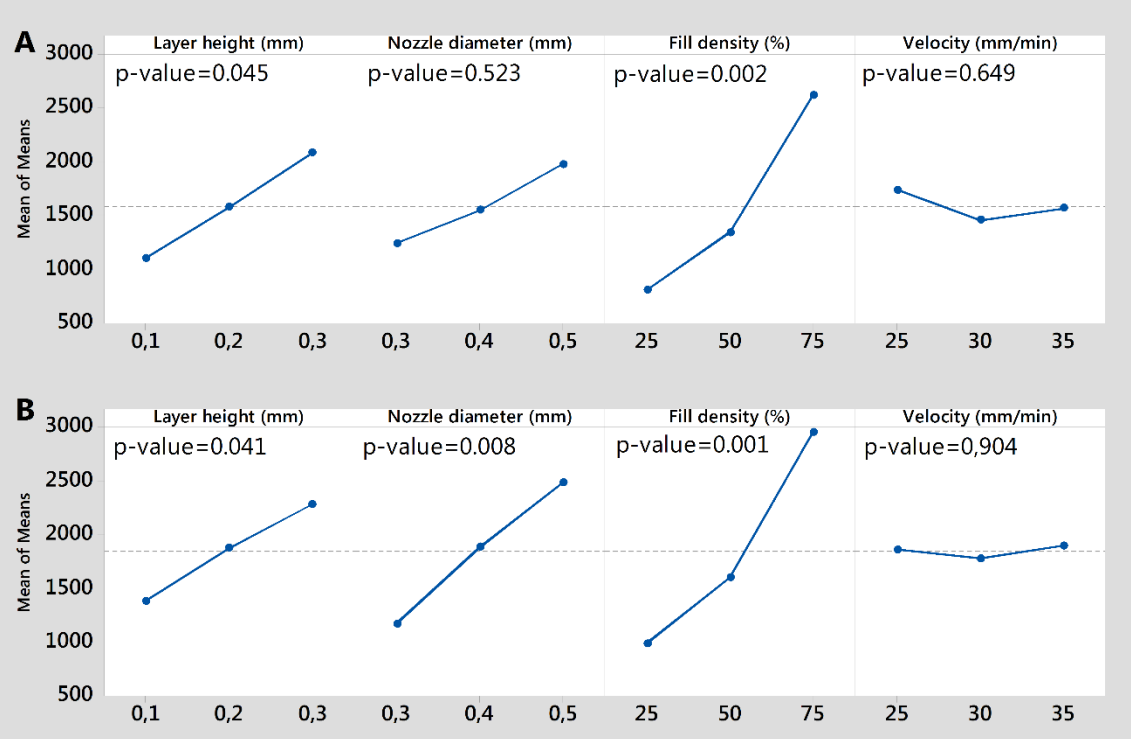

Fig. 6 Main effects plot for the response variable number of cycles to failure **A.** Rectilinear infill. **B.** Honeycomb infill

Interactions between layer height, nozzle diameter and fill density were also assessed through the ANOVA. Only the interaction nozzle diameter – layer height proved to be influential considering a 5% confidence level, as shows Fig. 7. According to that figure, selecting too high layer heights for parts manufactured with high-diameter nozzles can be counterproductive in terms of expected fatigue life, probably because cohesion forces between layers are harmed. More specifically, results show than the combination 0.4-mm nozzle and 0.3-mm layer height derives in no significant improvement with regards to the 0.2-mm layer height level. On the contrary, when the nozzle diameter is increased to 0.5 mm, that step even harms the expected cycles to failure. Therefore, if a nozzle of higher diameter wants to be used to increase productivity, layer height should not be significantly increased so not to be detrimental to expected life of the part. A minimum ratio of 1:1.5 of nozzle diameter/layer height is therefore advised.

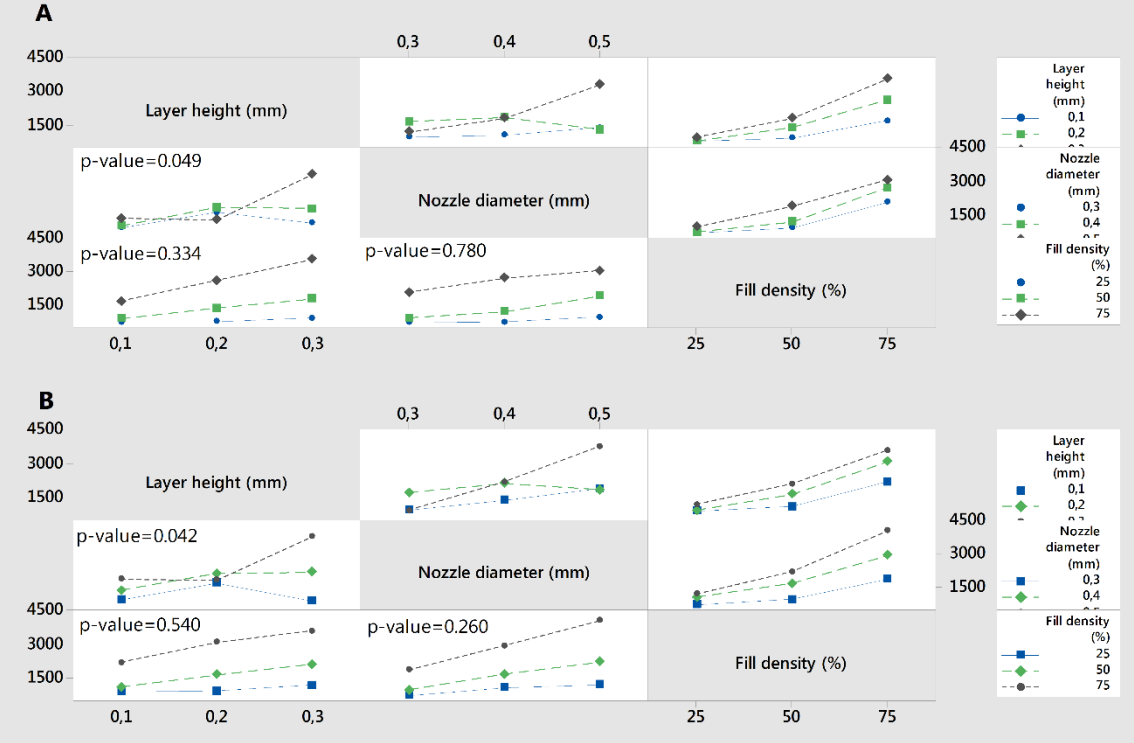

Fig. 7 Interactions plot for the response variable number of cycles to failure **A.** Rectilinear infill. **B.** Honeycomb infill.

3.3 Fractography

Different pictures of the specimen broken areas after the fatigue tests have been taken with a MOTIC SMC binocular loupe equipped with a MOTICAM 3 digital camera. The following figures show singular specimens that have been found interesting to illustrate the fracture process, and to compare both infills. In all cases, the crack begins around the area near the first or the last printed layer, as can be observed in Fig. 8A. This fact implies that the fibers that compose the curvature of the specimen act as concentrators,

from which all cracks are nucleated, and then propagated inside the specimen section. In the specimens printed with a rectilinear infill pattern and 75% (Fig. 8B), the failure shows a ductile behavior during its first stage (Fig. 8C). Then, the piece ends up breaking with a brittle break by fragile shear stress, as can be seen in the detail of Fig. 8D.

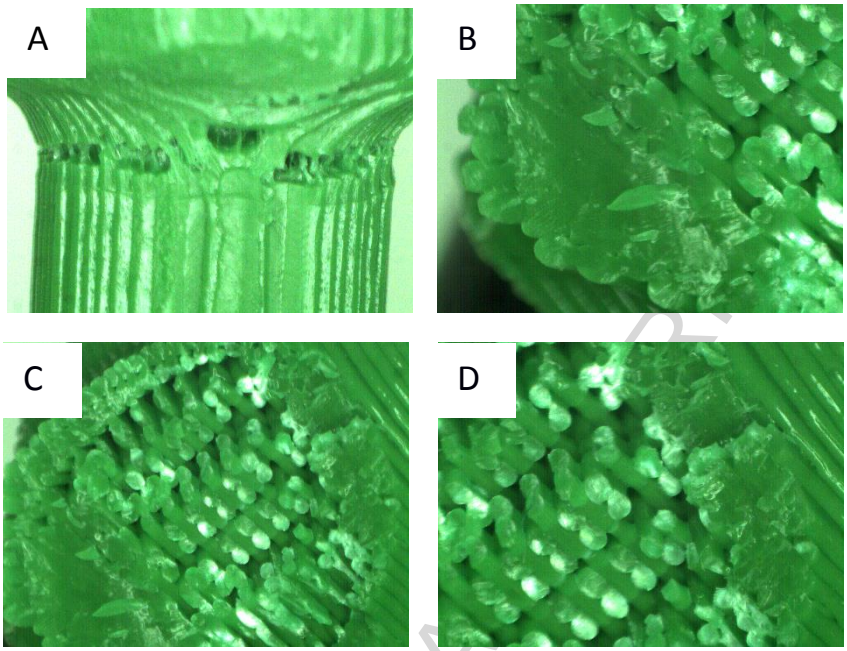

Fig. 8 Fractographies of specimen printed rectilinear infill pattern at 75% of infill. A- Crack initiation at outer layers. B- Section after fracture. C- Detail of ductile fracture area. D- Detail of fracture by shear stress.

In the specimens printed with the honeycomb infill pattern at 75% of infill, the fracture is fragile over the entire surface (Fig. 9A) and fatigue marks are easily observed in the detail picture represented in Fig. 9B.

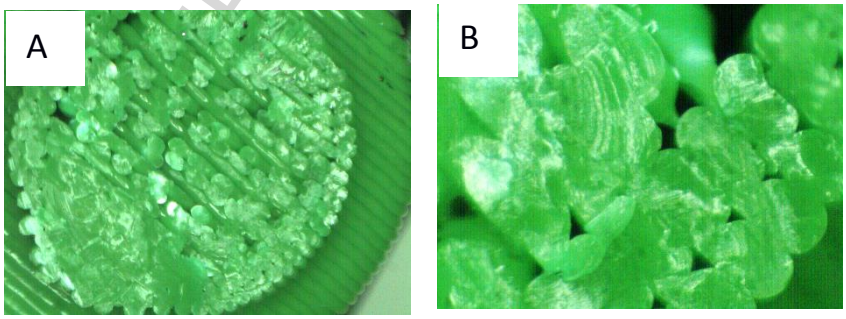

Fig. 9 Fractographies of specimen printed honeycomb infill pattern at 75% of infill. A- Fragile fracture area. B- Fatigue marks observed at outer fibers.

For the sake of comparison, specimens manufactured with a 25% infill present a ductile break on their outer layers, whereas the core fibers show fragile rupture (Figs. 10A and 10B). This behavior can be explained by the fact that the higher availability of space among filaments allow the outer layers to deform plastically before breaking.

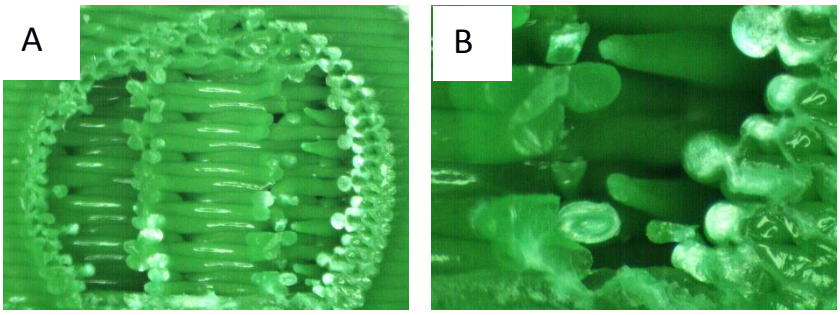

Fig. 10 Pictures of the specimen printed with honeycomb infill pattern at 25% of infill. A- General view of the section. B- Detail of void space between filaments in the fracture section.

These observations justify the information provided in section 3.3. The pieces printed with infill 75% and honeycomb are those that present greater area with fatigue tracks, and, therefore, slow down advance of the crack, which makes their fatigue life longer. Crack propagation as a combination of bending and shear stress defines the failure mode of this kind of specimens, as was already discussed by other authors [37].

3.4 Wöhler curve for optimal printing conditions

The analyzed results lead to the conclusion that there is an optimal combination of parameters in the defined DOE, which are summarized at Table 3. This set of conditions has been taken to print a second set of specimens, which have been then tested subjected to different levels of force. Table 4 shows the six different levels of force and the maximum bending stress to which the specimen is subjected in the stress concentrator area, calculated from the maximum bending moment.

Table 3 Optimal combination of factors and levels to maximize the expected cycles to failure.

Parameter	Layer height
Infill pattern	Honeycomb
Fill density	75%
Nozzle diameter	0.5 mm
Layer height	0.3 mm

Table 4 Forces applied for the Wöhler curve tests and maximum stress levels.

F (N)	M_{max} (N·mm)	σ_{max} (MPa)

10	1040	35.8
13	1352	46.6
15	1560	53.8
18	1872	64.5
20	2080	71.7
22	2288	78.8

With this data, different fatigue tests to construct the Wöhler curve were carried out at each of the indicated stress levels [38]. Following the protocol stablished by [39], three repetitions have been performed for each stress level, except for 53.8 MPa, is the already tested stress for the results of the DOE analysis.

The least-squares regression model used is according to equation (1)

$$y = A + Bx \quad (1)$$

Where the estimated values of *A* and *B* are

$$A = \bar{y} + B\bar{x} \quad (2)$$

$$B = \frac{\sum_{i=1}^{n_s}(x_i - \bar{x})(y_i - \bar{y})}{\sum_{i=1}^{n_s}(x_i - \bar{x})^2} \quad (3)$$

Where n_s is the number of test specimens, $\bar{x}$ and $\bar{y}$, are the average values of x and y

The S-N equation in logarithms form is (4).

$$\log(2N_f) = -\frac{1}{b}\log(S_f) + \frac{1}{b}\log(S_a) \quad (4)$$

Comparing equations (1) and (4), $x = \log(S_a)$ the independent variable; $y = \log(2N_f)$ the dependent variable, coefficient $B = \frac{1}{b}$ and coefficient $A = -\frac{1}{b}\log(S_f)$. Thus, the S-N curve equation is (5)

$$S_a = S_f(2N_f)^b \quad (5)$$

A potential curve, corresponding to equation (5), is deduced from the testing, with a R^2=0.9754, and represented in Fig. 11. Furthermore, the model used in this figure is only valid for the low cycle fatigue domain. According to the tests carried out, the specimens subjected to a maximum stress of 35.8 MPa did not experience failure before 10^5 cycles,

which allows us to establish this value as a lower threshold of the endurance limit. This value cannot be represented in the curve, since the specimens have not broken.

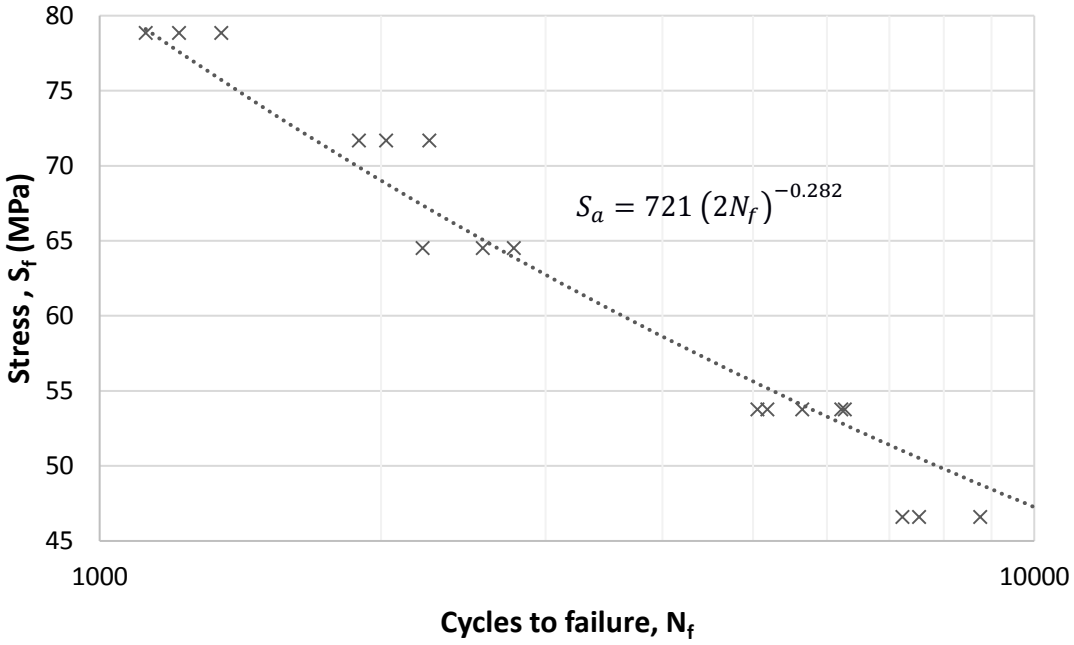

Fig. 11 Wöhler curve for specimens manufactured with honeycomb infill, 75% infill density, 0.5-mm diameter nozzle and 0.3 mm layer height.

4. Conclusions

The influence of fill density and pattern, nozzle diameter, layer height and printing speed on fatigue performance of cylindrical specimens has been studied through a Taguchi DOE. The following conclusions can be stated:

1. Fill density shows the highest influence in fatigue performance, followed by nozzle diameter and layer height, whereas printing speed shows no relevant influence in PLA specimens.
2. The honeycomb infill pattern is advised to manufacture FDM parts, as it enables a longer lifespan with regards to specimens manufactured using a rectilinear infill, requiring the same approximate manufacturing time.
3. A combination of 75% infill density, 0.5 mm nozzle diameter and 0.3 mm layer height results in the highest fatigue life.For that combination of factors, a lower threshold for the fatigue endurance limit has been found at 35.8 MPa.
4. The interaction between the nozzle diameter and layer height shows that using similar nozzle dimeter and layer height values derives in a detrimental fatigue performance of the part due to inappropriate deposition of material. The nozzle diameter should be, at least, 1.5 times the value of layer height to ensure proper cohesion between filaments for an enhanced part integrity.

5. A combination of brittle and ductile fracture patters has been found in the different specimens. In all cases, the fracture crack starts in the outer layers of the specimens, where the geometrical stress concentrator is found. This fact evidences the need of finishing the outer layers of parts as a mean of enhancing their fatigue behavior.
6. No thermal effect has been observed in the failure of PLA parts due to oscillating stresses.

References

1. R. Jerez-Mesa, J.A. Travieso-Rodriguez, X. Corbella, R. Busqué, G. Gomez-Gras, Finite element analysis of the thermal behavior of a RepRap 3D printer liquefier, Mechatronics, 36 (2016) 119-126.
2. R. Jerez-Mesa, G. Gomez-Gras, J.A. Travieso-Rodriguez, V. Garcia-Plana, A comparative study of the thermal behavior of three different 3D printer liquefiers, Mechatronics (2017) (in press).
3. C. Bellehumeur, L. Li, Q. Sun, P. Gu, Modeling of Bond Formation Between Polymer Filaments in the Fused Deposition Modeling Process, Journal of Manufacturing Processes, 6-2 (2004) 170-178.
4. M. Domingo-Espin, J.M. Puigoriol-Forcada, A.A. Garcia-Granada, J. Llumà, S. Borros, G. Reyes, Mechanical property characterization and simulation of fused deposition modeling Polycarbonate parts, Materials & Design, 83 (2015) 670-677.
5. Q. Sun, G.M. Rizvi, C.T. Bellehumeur, P. Gu, Effect of processing conditions on the bonding quality of FDM polymer filaments, Rapid Prototyping Journal, 14-2 (2008) 72-80.
6. P. Gurrala, S. Regalla, Part strength evolution with bonding between filaments in fused deposition modelling, Virtual and Physical Prototyping, 9-3 (2014) 141-149.
7. R.W. Gray, D.G. Baird, J. Helge Bøhn, Effects of processing conditions on short TLCP fiber reinforced FDM parts, Rapid Prototyping Journal, 4-1 (1998) 14-25.

8. W. Zhong, F. Li, Z. Zhang, L. Song, Z. Li, Short fiber reinforced composites for fused deposition modeling, Materials Science and Engineering: A, 301-2 (2001) 125-130.
9. F. Wang, L. Shor, A. Darling, S. Khalil, W. Sun, S. Güçeri, A. Lau, Precision extruding deposition and characterization of cellular poly-ε-caprolactone tissue scaffolds, Rapid Prototyping Journal, 10-1 (2004) 42-49.
10. A.K. Sood, R.K. Ohdar, S.S. Mahapatra, Parametric appraisal of mechanical property of fused deposition modelling processed parts, Materials and Design, 31-1 (2010) 287-295.
11. A. Bellini, S. Güçeri, Mechanical characterization of parts fabricated using fused deposition modeling, Rapid Prototyping Journal, 9-4 (2003) 252-264.
12. R. Quintana, J.W. Choi, K. Puebla, R. Wicker, Effects of build orientation on tensile strength for stereolithography-manufactured ASTM D-638 type I specimens, International Journal of Advanced Manufacturing Technology, 46-1 (2010) 201-215.
13. R. Hague, S. Mansour, N. Saleh, R. Harris, Materials analysis of stereolithography resins for use in Rapid Manufacturing, Journal of Materials Science, 39-7 (2004) 2457-2464.
14. U. Ajoku, N. Saleh, N. Hopkinson, R. Hague, P. Erasenthiran, Investigating mechanical anisotropy and end-of-vector effect in laser-sintered nylon parts, Proceedings of the Institution of Mechanical Engineers, Part B: Journal of Engineering Manufacture, 220-7 (2006) 1077-1086.
15. D.C. Thompson, R.H. Crawford, Computational quality measures for evaluation of part orientation in freeform fabrication, Journal of Manufacturing Systems, 16-4 (1997) 273-289.
16. I. Gibson, D. Shi, Material properties and fabrication parameters in selective laser sintering process, Rapid Prototyping Journal, 3-4 (1997) 129-136.

17. C. Majewski, N. Hopkinson, Effect of section thickness and build orientation on tensile properties and material characteristics of laser sintered nylon-12 parts, Rapid Prototyping Journal, 17-3 (2011) 176-180.
18. D. Olivier, D., J.A. Travieso-Rodriguez, S. Borros, G. Reyes, R. Jerez-Mesa, Influence of building orientation on the flexural strength of laminated object manufacturing specimens, Journal of mechanical science and technology, 31-1 (2017) 133-139.
19. K. Schmidtke, F. Palm, A. Hawkins, C. Emmelmann, Process and Mechanical Properties: Applicability of a Scandium modified Al-alloy for Laser Additive Manufacturing, Physics Procedia, 12 (2011) 369-374.
20. G. Berti, L. D'Angelo, A. Gatto, L. Luliano, Mechanical characterisation of PA-Al_2O_3 composites obtained by selective laser sintering, Rapid Prototyping Journal, 16-2 (2010) 124-129.
21. A.K. Sood, R.K. Ohdar, S.S. Mahapatra, Experimental investigation and empirical modelling of FDM process for compressive strength improvement, Journal of Advanced Research, 3-1 (2012) 81-90.
22. R. Singh, Some investigations for small-sized product fabrication with FDM for plastic components, Rapid Prototyping Journal, 19-1 (2013) 58-63.
23. I. Durgun, R. Ertan, Experimental investigation of FDM process for improvement of mechanical properties and production cost, Rapid Prototyping Journal, 20-3 (2014) 228-235.
24. L. Wahl, S. Maas, D. Waldmann, A. Zurbes, P. Freres, Shear stresses in honeycomb sandwich plates: Analytical solution, finite element method and experimental verification, Journal of Sandwich Structures and Materials, 14-4 (2012) 449-468.
25. T. Wang, J. Xi, Y. Jin, A model research for prototype warp deformation in the FDM process, International Journal of Advanced Manufacturing Technology, 33-11 (2007) 1087-1096.

26. R. Singh, Process capability analysis of fused deposition modelling for plastic components, Rapid Prototyping Journal, 20-1 (2013) 69-76.
27. M.A. Yardimci, S. Güçeri, Conceptual framework for the thermal process modelling of fused deposition, Rapid Prototyping Journal, 2-2 (1996) 26-31.
28. S. H. Ahn, M. Montero, D. Odell, S. Roundy, P.K. Wright, Anisotropic material properties of fused deposition modeling ABS, Rapid Prototyping Journal, 8-4 (2002) 248-257.
29. B.H. Lee, J. Abdullah, Z.A. Khan, Optimization of rapid prototyping parameters for production of flexible ABS object, Journal of materials processing technology, 169-1 (2005) 54-61.
30. A.B. Spierings, Fatigue performance of additive manufactured metallic parts, Rapid Prototyping Journal, 19-2 (2013) 88-94.
31. P. Edwards, M. Ramulu, Fatigue performance evaluation of selective laser melted Ti-6Al-4V, Materials Science and Engineering: A, 598 (2014) 327-337.
32. A. Riemer, S. Leuders, M. Thöne, H.A. Richard, T. Tröster, T. Niendorf, On the fatigue crack growth behavior in 316L stainless steel manufactured by selective laser melting, Engineering Fracture Mechanics, 120 (2014) 15-25.
33. M.F. Afrose, S. H. Masood, P. Iovenitti, M. Nikzad, I. Sbarski, Effects of part build orientations on fatigue behaviour of FDM-processed PLA material. Progress in Additive Manufacturing, 1-1 (2016) 21-28.
34. O.A. Mohamed, S.H. Masood, J.L. Bhowmik, Optimization of fused deposition modeling process parameters: a review of current research and future prospects, Advances in Manufacturing, 3-1 (2015) 42-53.
35. G. Taguchi, S. Chowdhury, Y. Wu, Taguchi's quality engineering handbook. Hoboken, NJ: John Wiley & Sons, 2005.
36. ASTM, D7774-12, Standard Test Method for Flexural Fatigue Properties of Plastics, D20.10.24, Ed. West Conshohocken, PA, ASTM International (2013).

37. F.S. Senatov, K.V. Niaza, A.A. Stepashkin, S.D. Kaloshkin, Low-cycle fatigue behavior of 3d-printed PLA-based porous scaffolds. Composites Part B: Engineering, 97 (2016) 193-200.
38. Y.L. Lee, J. Pan, R.B. Hathaway, M.E. Barkey, Fatigue testing and analysis: theory and practice, Elsevier Butterworth-Heinemann, 13 (2005).
39. P.H. Wirsching, M.C. Light, Fatigue under wide band random stresses, Journal of the Structural Division, 106-7 (1980) 1593-1607.

Graphical abstract

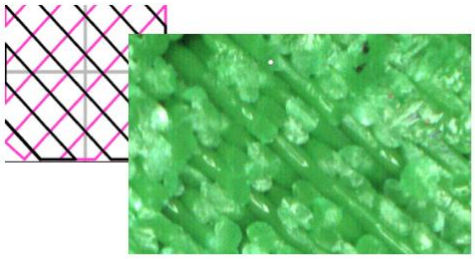

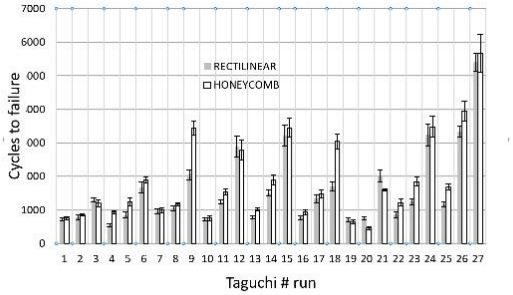

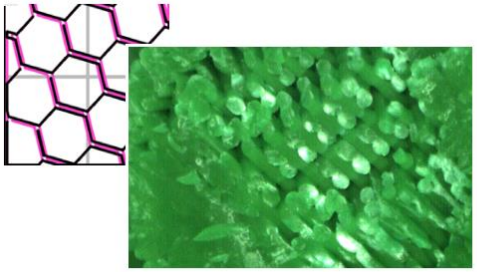

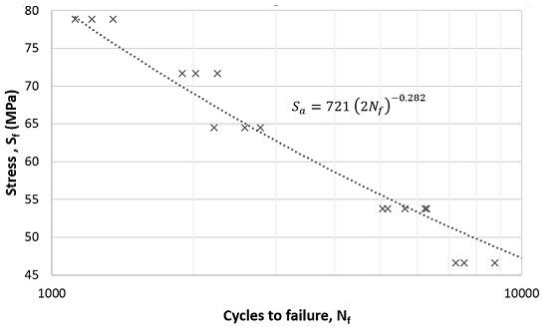

Highlights

- Taguchi experimental design has been applied to analyze fatigue of PLA parts
- The optimal set of parameters resulting in the highest number of cycles to failure was found
- Fill density is the most influential parameter on fatigue life, followed by layer height
- The Wöhler curve for the optimal set of parameters have been represented
- Crack nucleation and propagation have been observed through optical microscopy